sciendo

Int. J. Appl. Math. Comput. Sci., 2025, Vol. 35, No. 3, 429–442
DOI: 10.61822/amcs-2025-0030

amcs

FAULT DETECTION BASED ON INTERVAL OBSERVERS AND DYNAMIC EVENT–TRIGGERED FAULT–TOLERANT CONTROL FOR MORPHING AIRCRAFT

XINGJIAN FU [a,*], XIAOHAN WANG [a]

[a]School of Automation
Beijing Information Science and Technology University
No. 12, Xiaoying East Road, Haidian District, Beijing, China
e-mail: fxj@bistu.edu.cn, wwxxhh981118@163.com

In this paper, a fault detection mechanism using interval observers and a robust fault-tolerant control strategy with dynamic event-triggered mechanism are designed for the switched control problem during the transformation process of a morphing aircraft. Firstly, an interval observer design method for the nonlinear switched system is given. It is converted by coordinate transformation into the form of solving Sylvester's equation in the absence of actuator faults. Secondly, by using the output of the interval observer, the upper and lower bounds of the system output under the no actuator faults condition are constructed, and the design of the fault detection mechanism is achieved by monitoring whether the system output exceeds the bounds. Thirdly, in order to save communication resources, a robust fault-tolerant control strategy based on dynamic event-triggered mechanism is designed. Based on fault detection results, two different controllers are utilized for switched control, ensuring the boundedness of the closed-loop system signal, and conditions for the asymptotic stability of the closed-loop system are offered. Finally, a nonlinear model of morphing aircraft system with variable wing curvature is used to verify the validity of the designed scheme.

Keywords: morphing aircraft, interval observer, fault detection, dynamic event-triggered, robust fault-tolerant control, switched system.

1. Introduction

With the rapid development of aviation technology, traditional aircrafts are gradually showing their limitations in carrying out complex and diversified missions. These aircrafts typically have fixed aerodynamic configurations that cannot be adapted to changing flight environments and mission requirements. As a result, the concept of the morphing aircraft has emerged. It enables the aircraft to adjust its morphology to maintain an optimal flight state according to different flight environments and mission needs by changing its aerodynamic configuration during flight, such as variable wingspan, variable swept-back wing, etc. (Dong *et al*., 2015; Wu *et al*., 2017). However, as the morphing aircraft is a complex nonlinear switched system with serious external disturbances in its transformation process, researchers mostly adopt the idea of combining several control methods. This leads to its controller design process appears to be exceptionally difficult.

Switched systems, as a hybrid system, can be modelled for many engineering applications due to the presence of various jump parameters. However, the study of switched systems is made difficult by the fact that their dynamics depend on the subsystems'h dynamics and switching signals. This makes it difficult to study the stability of these systems. In order to address this issue, methods such as common Lyapunov functions, multiple Lyapunov functions, and the average dwell time method have been proposed by researchers for studying the stability of switched systems under arbitrary or constrained switching signals (Meng *et al*., 2020; Wang *et al*., 2019; Zhao *et al*., 2011). The theory of switched systems provides an effective way in the problem of designing control systems for morphing aircrafts (Ligang *et al*., 2020; Liang *et al*., 2019). Q-learning based switched control strategies for variable swept wing

*Corresponding author

© 2025 X. Fu and X. Wang.
This is an open access article distributed under
the Creative Commons Attribution-NonCommercial-NoDerivs license
(http://creativecommons.org/licenses/by-nc-nd/4.0/).

deformable aircraft are investigated by Ligang *et al*. (2020). The relevant altitude motion model is established and the inner and outer two-part controllers are designed to learn the optimal commands through the Q-learning algorithm. Liang *et al*. (2019) establish a longitudinal short-period linear switched model of a morphing aircraft by combining with the theory of switched system to address the control problem of the morphing aircraft during its transformation process. An improved robust adaptive control law is designed to suppress the effects of various kinds of disturbances and uncertainties on the system.

Nowadays, the research on nonlinear systems turns to various practical scenarios. Event-triggered control (ETC) is one of the important directions. It has attracted much attention from researchers due to its ability to reduce computational cost and communication resources while maintaining satisfactory system performance (Wu *et al*., 2021; Ma *et al*., 2020; Ding *et al*., 2019). Since the application fields of switched systems are very wide and most of them rely on networks for information transmission, networked control inevitably has the problems of limited bandwidth and additional occupied communication resources. Therefore, it is especially necessary to introduce event-triggered mechanism in switched system (Liu *et al*., 2019; Lian and Li, 2021). In the work of Liu *et al*. (2019), the problem of fault detection in network switched control systems subject to repetitive scalar nonlinearities and random perturbations under an event-triggered scheme is considered. A nonlinear fault detection filter is proposed to generate residual signals and detect system faults, and an event-triggered strategy is applied to limit the signal transmission.

Compared to static event-triggered mechanism, in order to further reduce the consumption of communication resources, a dynamic event-triggered mechanism is proposed by Girard (2014) as well as Xia and Fu (2024). That is, internal dynamic variables are added to the static event triggered conditions. In this way, a larger trigger interval and fewer triggers can be obtained under the premise of ensuring system performance. Currently, many researchers have studied the application of event-triggered mechanisms, and the research results are quite abundant. Event-triggered mechanisms are widely used in dealing with various types of problems (Li *et al*., 2021; Long *et al*., 2022; Wan *et al*., 2021). The transient H_∞ tracking performance of switching linear variable parameter (LPV) aero-engine models over a limited time range is investigated using a dynamic event triggered method by Li *et al*. (2021). By constructing a novel dynamic event-triggered mechanism, the transmission interval can be dynamically adjusted according to the changes in tracking performance, which greatly reduces the transmission cost. In the work of Long *et al*. (2022) robust adaptive event-triggered control of nonlinear switched systems is investigated. The robust adaptive controller under dwell time switching is designed by backstepping method. And the event-triggered mechanism is integrated into the switched controller, which can effectively avoid zeno behavior and ensure the global asymptotic stability of the system. Wan *et al*. (2021) investigate fault detection and isolation under the dynamic event triggered mechanism for switched systems and propose an improved dynamic event triggering mechanism. Also the dynamic event triggered mechanism is improved, which contains two internal dynamic variables, mode information and seven adjustable parameters. Therefore, the data transmission can be flexibly adjusted to save network resources.

In the last decade, fault-tolerant control has made significant advances in the design and implementation of control strategies and mechanisms capable of maintaining stability in the event of system failures or errors. These advances are largely based on the design of an integrated fault diagnosis and compensation architecture (FDA). The architecture typically employs fault detection, isolation and estimation (FDIE) mechanisms to provide relevant fault information for the design of the controller (Abbaspour *et al*., 2017; Avram *et al*., 2017). In the work of Abbaspour *et al*. (2017) sensor and actuator fault identification control for unmanned aerial vehicles (UAVs) using a neural adaptive observer is investigated using an extended Kalman filter to reconstruct the parameters. Avram *et al*. (2017) design a fault diagnosis architecture consisting of a nonlinear fault estimator and a set of nonlinear adaptive fault isolation estimators based on the functional structure of the fault. After isolating the faults, the fault parameter estimates generated by the matched isolation estimators are used to adapt and compensate for the effects of the faults.

Due to the ever-increasing complexity of industrial systems, the fault of any single component can lead to serious damage or even catastrophic consequences. Therefore, fault detection techniques are essential in improving the safety and reliability of the system and in preventing faults from occurring. Early fault detection relied heavily on hardware redundancy, which had the advantage of high reliability and the ability to isolate faults directly. However, due to high cost and space constraints, this method is no longer applicable in modern control systems. As a result, analytical redundancy-based fault detection methods have emerged, which can be broadly classified into model-based (Habibi *et al*., 2019; Junnila and Laihonen, 2020), signal processing-based (Germán-Salló and Strnad, 2018) and observer-based (Ashraf *et al*., 2021; Li *et al*., 2019) fault detection methods. The observer is widely used as an effective residual generator for fault detection. An adaptive fault/state observer with H_∞ performance is proposed

by Ashraf *et al*. (2021) to estimate actuator and sensor faults simultaneously. To implement the tracking control a nonlinear sliding mode state feedback control law is designed based on the estimated state and fault information of the fault estimation unit. In the work of Li *et al*. (2019), the problem of fault detection and fault estimation for DC-DC conversion based switching systems is mainly investigated. Fault detection is achieved by designing a sliding mode observer (SMO) to generate residual signals, comparing them with a predetermined threshold, and fault estimation is achieved by using fault reconstruction methods.

With the rise of interval observer theory, new ideas for fault detection have been provided (Guo *et al*., 2019; Guo and Zhu, 2016a; Yang and Zhang, 2018). By constructing upper and lower bounds of the observer, the interval observer provides a limit for the dynamic change of the state and a natural threshold for fault diagnosis. The two links of designing residual evaluator and threshold selector are omitted in the traditional observer-based fault diagnosis method, and the method is concise and intuitive. In the work of Guo *et al*. (2019), for generalized systems containing actuator faults, a methodology to achieve fault detection using interval observers is investigated. Guo and Zhu (2016a) utilize an interval observer to construct the corresponding residuals, and propose a fault detection method for nonlinear systems with both uncertainty and external disturbances and containing actuator faults.

Based on the above analysis, a fault detection mechanism based on interval observer and a robust fault-tolerant control problem based on dynamic event-triggered mechanism are investigated for the morphing aircraft system. The main contributions of this paper can be summarized as follows:

(i) Fault detection for a morphing aircraft system in the presence of external disturbances, actuator faults, and uncertainties is achieved by designing an interval observer.

(ii) A robust fault-tolerant controller based on the dynamic event-triggered mechanism is constructed, and the conditions for the closed-loop system to be asymptotically stable are given, and the Zeno behavior is excluded. According to the results of fault detection, the switched control with two different controllers can ensure the boundedness of the signal of the closed-loop system and greatly reduce the number of communications.

(iii) The validity of the scheme is verified by nonlinear simulation of the morphing aircraft system with variable wing curvature used in the literature (Zhu and Yu, 2022).

Based on the above analysis, the present paper makes the following main contributions:

(i) In order to visualize real-time fault information,a novel fault detection mechanism is introduced that employs interval observers for nonlinear switched systems, allowing intuitive fault identification by monitoring whether the system output exceeds predefined bounds.

(ii) To solve the difficult problem of communication resource efficiency in fault-tolerant control, a dynamic event-triggered robust fault-tolerant control strategy is proposed. Based on the real-time fault detection results obtained from the interval observer, different controllers can be used for switching control by the strategy, which effectively reduces data transmission while ensuring that the signal of the closed-loop system is bounded.

(iii) The effectiveness of the designed fault detection mechanism and fault-tolerant control method is verified through modeling and simulation of a morphing aircraft system with variable wing curvature, providing theoretical support for practical applications.

2. Modelling and analysis of the morphing aircraft

Morphing aircraft with variable wing curvature is considered in this paper. The longitudinal periodic nonlinear dynamics of the morphing aircraft is expressed as follows (Zhu and Yu, 2022):

$$\begin{cases} mV\dot{\gamma} = \tilde{T}\sin\alpha + L_f - mg\cos\gamma - F_{I_z}, \\ mV\dot{\alpha} = -\tilde{T}\sin\alpha - L_f + mg\cos\gamma + F_{I_z} + mVq, \\ \dot{q} = -\frac{\dot{I}_y}{I_y}q + \frac{1}{I_y}\left(-S_x g\cos\theta + M_A + \tilde{T}Z_T + M_{I_y}\right), \\ \dot{\theta} = q, \end{cases} \tag{1}$$

where m is the mass of the aircraft, V is the flight speed, γ is the trajectory angle, q is the pitch angle speed, θ is the pitch angle, $\tilde{T}$ is the thrust, α is the angle of approach, g is the gravitational acceleration, I_y is the rotational moment of inertia of the aircraft around the y-axis of the fuselage, Z_T is the power position, L_f is the lift, M_A is the aerodynamically generated pitching moment, and M_{I_y} is the moment of inertia induced by the body-change process.

Defining $\bar{x}_f$ as the distance from the leading edge vertex at the wing's maximum curvature, and $\bar{y}_c(\bar{x})$ as the wing curvature distribution function with a maximum value of relative curvature $\bar{c}$, one can get

$$\bar{y}_c(\bar{x}) = 0.5(\bar{y}_{up} + \bar{y}_{down}), \tag{2}$$

$$\bar{c} = \frac{c}{r} = [\bar{y}_c(\bar{x})]_{\max}, \tag{3}$$

$$\bar{x}_f = \frac{x_f}{r}, \tag{4}$$

where $\bar{y}_{up}$ denotes the perpendicular distance of the upper surface of the airfoil with respect to the chord line and $\bar{y}_{down}$ denotes the perpendicular distance of the lower surface of the airfoil with respect to the chord line. The distribution of the two in the chord length direction together defines the thickness and shape characteristics of the airfoil.

Using the small disturbance linearization method to linearize the system (1) at the equilibrium point, the state matrix A and control matrix B can be obtained:

$$A = \begin{bmatrix} -2\dfrac{Q_0 S_W C_{D0}}{\mathrm{m}V_0} & \dfrac{Q_0 S_W (C_{L0} - C_{D\alpha})}{m} & -g & 0 \\ -2\dfrac{Q_0 S_W C_{L0}}{\mathrm{m}V_0} & -\dfrac{Q_0 S_W (C_{D0} + C_{L\alpha})}{m} & 0 & 1 \\ 0 & 0 & 0 & 1 \\ 2\dfrac{Q_0 S_W c_A C_{M0}}{I_y V_0} & \dfrac{Q_0 S_W c_A C_{M\alpha}}{I_y} & 0 & 0 \end{bmatrix}, \tag{5}$$

$$B = \begin{bmatrix} 0 & \dfrac{T_{\delta T}}{m} \\ -\dfrac{Q_0 S_W C_{L\delta e}}{\mathrm{m}V_0} & 0 \\ 0 & 0 \\ \dfrac{Q_0 S_W c_A C_{M\delta e}}{I_y} & 0 \end{bmatrix}. \tag{6}$$

V_0 , Q_0 , S_W , C_{D0} , C_{L0} , C_{M0} , $C_{M\delta e}$, $T_{\delta T}$, c_A are the flight speed of the morphing aircraft at the equilibrium point, the dynamic pressure, the wing reference area, the lift coefficient, the drag coefficient, the pitching moment coefficient, the lift coefficient of the elevator, the moment coefficient of the elevator, the thrust coefficient of the engine, and the mean aerodynamic chord length of the wing, respectively. By substituting the fitted aerodynamic parameters with the wing curvature function, the equation of state of the morphing aircraft containing the parameter (wing curvature c) is obtained

$$\dot{X} = A(c)X + BU, \tag{7}$$

where the state variables

$$X = \begin{bmatrix} \Delta V & \Delta\alpha & \Delta\theta & \Delta q \end{bmatrix}^T$$

represent velocity (m/s), angle of attack (rad), pitch angle (rad) and pitch angle speed (rad/s), respectively. The control input variables $U = \begin{bmatrix} \Delta\delta_e & \Delta\delta_{\tilde{T}} \end{bmatrix}$ represent the elevator deflection angle and throttle opening, respectively. Based on the functional relationship between fitted aerodynamic parameters and curvature, the variable parameter matrix model containing the varying parameter (curvature c) can be obtained by substituting the state matrix A (Zhu and Yu, 2022):

$$A(c) = \begin{bmatrix} -0.0003282c - 0.00246 & 3.08c - 3.903 & -9.8 & 0 \\ -0.0003766c - 0.000067 & -0.000164c - 0.9465 & 0 & 1 \\ 0 & 0 & 0 & 1 \\ 0.00821c + 0.005878 & -4.6677 & 0 & 0 \end{bmatrix}, \tag{8}$$

where $A(c)$ is the state matrix of the morphing aircraft model with the wing curvature change parameter c. The aircraft increases the wing curvature c by increasing the thickness of the upper surface of the wing, and the change of the state quantity caused by the wing curvature c changes the flight state.

Based on the theory of switched systems, the transformation process of the wing curvature of an aircraft can be described as a linear switched system:

$$\dot{x}(t) = A_\sigma x(t) + B_\sigma u(t). \tag{9}$$

If the uncertainties, disturbances and actuator faults of the wing curvature during switching are considered, the following nonlinear switched system can be constructed:

$$\begin{cases} \dot{x}(t) = A_\sigma x(t) + B_\sigma u(t) + E_\sigma S(t) \\ \qquad\quad + f_\sigma(x,t) + D_\sigma \omega(t), \\ y(t) = C_\sigma x(t), \end{cases} \tag{10}$$

where $\sigma : R^+ \to N\{1, 2, \cdots, n\}$ is the switching signal, which is a segmented constant-value function dependent on state or time. $y(t), u(t), x(t), S(t), \omega(t)$ represent output variables, input variables, state variables, actuator faults, and unknown external perturbations, respectively. $A_\sigma, B_\sigma, C_\sigma, D_\sigma, E_\sigma$ are matrices of known real constants of appropriate dimensions.

Assumption 1. For the initial state of the system $x(0)$, there exist known vectors $\bar{x}(0)$, $\underline{x}(0)$ that satisfy $\underline{x}(0) \leq x(0) \leq \bar{x}(0)$. For the unknown external disturbances $\omega(t)$, there exist known upper and lower bounds $\bar{\omega}(t)$, $\underline{\omega}(t)$ that satisfy $\underline{\omega}(t) \leq \omega(t) \leq \overline{\omega}(t)$.

Assumption 2. For any $\sigma \in N$, f_σ is a known nonlinear function that is monotonically increasing with respect to x and satisfies the global Lipschitz condition, for all $t \geq 0$, there are

$$||f_\sigma(x,t)|| \leq \theta ||x_1 - x_2||,$$

where θ is the known Lipschitz constant.

Assumption 3. (A_σ, B_σ) is controllable and (A_σ, C_σ) is observable.

Lemma 1. (Guo *et al.*, 2019) *For a vector $x \in R^n$,there exist known vectors $\bar{x}(t), \underline{x}(t) \in R^n$, such that $\underline{x}(t) \leq x(t) \leq \bar{x}(t)$, if $A \in R^{m\times n}$ is a non-negative matrix, then the following inequality holds*

$$A\underline{x}(t) - A\bar{x}(t) \leq Ax(t) \leq A\bar{x}(t) - A\underline{x}(t).$$

Lemma 2. (Cui and Xiang, 2022) *For any matrices A and B of appropriate dimensions, the following inequality holds*

$$A^TB + B^TA \leq \gamma A^TA + \frac{1}{\gamma}B^TB.$$

Lemma 3. (Ashraf *et al.*, 2021b) *For a scalar μ and a symmetric positive definite matrix $G > 0$, the following inequality holds*

$$2x^Ty \leq \frac{1}{\mu}x^TGx + \mu y^TG^{-1}y \quad x, y \in R.$$

Lemma 4. (Guo and Zhu, 2016a) *For a continuous system $\dot{x}(t) = Ax(t) + w(t)$, if $x(0) \geq 0$, then for $\forall t \geq 0$, there must be $x(t) \geq 0$, where $A \in R^{m\times n}$ is a Metzler matrix.*

Definition 1. (*Guo and Zhu, 2016b*) A square matrix *A* is said to be a Hurwitz matrix if all of its eigenvalues have negative real parts, and a Schur matrix if all of the eigenvalue norms of the square matrix *A* are less than one.

3. Design of an interval observer

Take $\psi(t) = Tx(t)$,T to be an invertible constant matrix. Let $S(t) = 0$, then system (10) can be rewritten as

$$\begin{cases} \dot{\psi}(t) = TA_\sigma T^{-1}\psi(t) + TB_\sigma u(t) \\ \qquad\quad +TD_\sigma\omega(t) + Tf_\sigma(t,x), \\ y(t) = CT^{-1}\psi(t). \end{cases} \tag{11}$$

Therefore, without considering the effect of actuator failure, the interval observer can be designed as

$$\begin{cases} \dot{\bar{\psi}}(t) = TA_\sigma T^{-1}\bar{\psi}(t) + TB_\sigma u(t) \\ \qquad +TL(y - CT^{-1}\bar{\psi}(t)) + (TD_\sigma)^+\bar{\omega}(t) \\ \qquad -(TD_\sigma)^-\underline{\omega}(t) + Tf_\sigma(t,\bar{x}) - Tf_\sigma(t,\underline{x}), \\ \dot{\underline{\psi}}(t) = TA_\sigma T^{-1}\underline{\psi}(t) + TB_\sigma u(t) \\ \qquad +TL(y - CT^{-1}\underline{\psi}(t)) + (TD_\sigma)^+\underline{\omega}(t) \\ \qquad -(TD_\sigma)^-\bar{\omega}(t) + Tf_\sigma(t,\underline{x}) - Tf_\sigma(t,\bar{x}), \end{cases} \tag{12}$$

where L is the observer gain matrix,

$$(TD)^+ = \max\{0, TD\}, (TD)^- = (TD)^+ - TD,$$

and it is easy to get $(TD)^+ \geq 0, (TD)^- \geq 0$.

Theorem 1. *If there exists a matrix L such that $\Psi = T(A - LC)T^{-1} \geq 0$ and is a Schur matrix, take $\underline{\psi}(0) = \min\{T\bar{x}(0), T\underline{x}(0)\}$, it $\bar{\psi}(0) = \max\{T\bar{x}(0), T\underline{x}(0)\}$. When $S(t) \equiv 0$, for $\forall t \geq 0$, there is*

$$\underline{\psi}(t) \leq \psi(t) \leq \bar{\psi}(t). \tag{13}$$

Then system (12) is an interval observer for system (10) without actuator faults.

Proof. Define the upper bound error of the interval observer

$$\bar{\tilde{\psi}}(t) = \bar{\psi}(t) - \psi(t). \tag{14}$$

One can get

$$\begin{aligned} \dot{\bar{\tilde{\psi}}}(t) &= TA_\sigma T^{-1}\bar{\psi}(t) + TB_\sigma u(t) + TL(y - CT^{-1}\bar{\psi}(t)) \\ &\quad + [(TD_\sigma)^+\bar{\omega}(t) - (TD_\sigma)^-\underline{\omega}(t)] + [Tf_\sigma(t,\bar{x}) \\ &\quad - Tf_\sigma(t,\underline{x})] - TA_\sigma T^{-1}\psi(t) - TB_\sigma u(t) \\ &\quad - TD_\sigma\omega(t) - Tf_\sigma(t,x) \\ &= T(A - LC)T^{-1}\bar{\psi}(t) + TLCT^{-1}\psi(t) \\ &\quad - TAT^{-1}\psi(t) + [(TD_\sigma)^+\bar{\omega}(t) - (TD_\sigma)^-\underline{\omega}(t)] \\ &\quad - TD_\sigma\omega(t) + [Tf_\sigma(t,\bar{x}) - Tf_\sigma(t,\underline{x}) - Tf_\sigma(t,x)] \\ &= T(A - LC)T^{-1}\bar{\tilde{\psi}}(t) + [(TD_\sigma)^+\bar{\omega}(t) \\ &\quad - (TD_\sigma)^-\underline{\omega}(t) - TD_\sigma\omega(t)] + [Tf_\sigma(t,\bar{x}) \\ &\quad - Tf_\sigma(t,\underline{x}) - Tf_\sigma(t,x)]. \end{aligned} \tag{15}$$

■

According to Assumption 1 and Lemma 1, it follows that

$$\begin{aligned} (TD)^-\underline{\omega}(t) \leq (TD)^-\omega(t) \leq (TD)^-\bar{\omega}(t), \\ (TD)^+\underline{\omega}(t) \leq (TD)^+\omega(t) \leq (TD)^+\bar{\omega}(t). \end{aligned} \tag{16}$$

According to (16), it is easy to obtain that

$$(TD_\sigma)^+\bar{\omega}(t) - (TD_\sigma)^-\underline{\omega}(t) - TD_\sigma\omega(t) \geq 0. \tag{17}$$

Under Assumption 2, there are

$$\begin{aligned} Tf_\sigma(t,\bar{x}) - Tf_\sigma(t,x) \geq 0, \\ Tf_\sigma(t,x) - Tf_\sigma(t,\underline{x}) \geq 0. \end{aligned} \tag{18}$$

It is easy to get

$$Tf_\sigma(t,\bar{x}) - Tf_\sigma(t,x) - Tf_\sigma(t,\underline{x}) \geq 0. \tag{19}$$

Since $\psi(t) = Tx(t)$, the initial state of system (11) satisfies

$$\underline{\psi}(0) \leq \psi(0) \leq \bar{\psi}(0), \tag{20}$$

i.e.,

$$\bar{\tilde{\psi}}(0) = \bar{\psi}(0) - \psi(0) \geq 0. \tag{21}$$

It follows from Lemma 4 that for any $t > 0$ it holds that

$$\tilde{\bar{\psi}}(t) = \bar{\psi}(t) - \psi(t) \geq 0. \tag{22}$$

Similarly, defining the lower bound error $\tilde{\underline{\psi}}(t) = \psi(t) - \underline{\psi}(t)$, for any $t \geq 0$, one can get

$$\tilde{\underline{\psi}}(t) = \psi(t) - \underline{\psi}(t) \geq 0. \tag{23}$$

Thus, for any $t \geq 0$, there is $\underline{\psi}(t) \leq \psi(t) \leq \bar{\psi}(t)$, and then (12) is said to be the interval observer of the system (10) in the absence of actuator faults.

Remark 1. Since T is an invertible matrix, the Sylvester equation can be constructed from $\Psi = T(A - LC)T^{-1}$ as follows:

$$TA - \Psi T = QC, TL = Q \tag{24}$$

where Ψ is usually chosen as a diagonal matrix, and the unique solutions L and T can be obtained by solving Eqn. (24) through MATLAB if and only if the matrix Ψ does not have common eigenvalues with matrix A.

The above interval observer is designed under the assumption that there is no actuator fault, i.e., $S(t) = 0$. In this case, the upper and lower bounds of the output of the interval observer can be defined as

$$\begin{cases} \bar{y}(t) = \max\{C_i T^{-1}\bar{\psi}(t), C_i T^{-1}\underline{\psi}(t)\}, \\ \underline{y}(t) = \min\{C_i T^{-1}\bar{\psi}(t), C_i T^{-1}\underline{\psi}(t)\}. \end{cases} \tag{25}$$

That is, the actual output of the system without actuator faults should satisfy $\underline{y}(t) \leq y(t) \leq \bar{y}(t)$. The observer output error is defined as $\bar{e}_y(t) = \bar{y}(t) - y(t), \underline{e}_y(t) = y(t) - \underline{y}(t)$. Based on this, an interval observer-based fault detection mechanism is designed as follows:

$$\begin{cases} if\ \underline{e}_y(t) > 0\ or\ \bar{e}_y(t) < 0\ \Rightarrow fault = 1 \Rightarrow alarm, \\ if\ \underline{e}_y(t) < 0\ or\ \bar{e}_y(t) > 0\ \Rightarrow fault = 0. \end{cases} \tag{26}$$

4. Design of a dynamic event-triggered robust fault-tolerant control method

In this section, the dynamic event-triggered conditions are given, and an internal dynamic variable is designed on the basis of the static event-triggered mechanism to obtain a longer trigger interval. The specific scheme adopted is as follows:

$$\begin{cases} t_0 = 0, \\ \tilde{t}_{k+1} = \inf\{t > t_k | \phi(t) + r_0 \\ \qquad + \partial(\varepsilon_1 ||\widehat{x}(t)|| - ||\widehat{e}(t)||) \leq 0\}, \end{cases} \tag{27}$$

where $\partial > 0, r_0 > 0, ||\widehat{x}(t)||$ is the paradigm term of the state $x(t)$. The dynamic variable $\phi(t)$ is defined as

$$\dot{\phi}(t) = -\chi\phi(t) + \varepsilon_1 ||\widehat{x}(t)|| - ||\widehat{e}(t)|| \tag{28}$$

Initial conditions are $\phi(0) \geq \phi_0, \chi > 0$. The event trigger error is defined as

$$\widehat{e}(t) = x(\tilde{t}_k) - x(\tilde{t}_{k+1}), \tag{29}$$

where $\tilde{t}_k$ is the event-triggered transient. The k-th event-triggered instant $\tilde{t}_k$ is recorded and controller parameters are updated when the triggering condition in (27) is satisfied.

Remark 2. By introducing a small fixed threshold r_0 to the dynamic event-triggered condition (27), it is ensured that the time interval between two consecutive events is non-negative and not infinitely close to 0. The frequency of event-triggered can be effectively reduced to avoid the occurrence of Zeno phenomenon. In this paper, it is considered that (27) will be applied to the robust fault-tolerant controller to be designed next, assuming that n samples occur on the interval, then

$$u(t) = \begin{cases} u(\tilde{t}_k), & t \in [t_i, \tilde{t}_{k+1}), \\ u(\tilde{t}_{k+1}), & t \in [\tilde{t}_{k+1}, \tilde{t}_{k+2}), \\ \vdots & \\ u(\tilde{t}_{k+n}), & t \in [\tilde{t}_{k+n}, t_{i+1}). \end{cases} \tag{30}$$

Based on the diagnostic results of the fault detection mechanism (26), the robust fault-tolerant control law for designing the nonlinear switched system (10) is defined as follows:

$$u(t) = \begin{cases} u_w(t) & \text{if } fault = 0, \\ u_w(t) + u_s(t) & \text{if } fault = 1. \end{cases} \tag{31}$$

The impact of disturbances and faults on the system is assessed by the fault detection mechanism. If the system is determined to be stable and its state trajectory is observed to remain within the range of the interval observer, the fault signal is set to $fault = 0$, i.e., $u(t) = u_w(t) = -K_i x(t)$, indicating that the system performance is not significantly affected by faults or disturbances. Conversely, if the state trajectory is found to deviate outside the observer's range due to a fault or disturbance, indicating a significant impact on system performance, the fault signal is set to $fault = 1$, i.e., $u(t) = u_w(t) + u_s(t) = -K_i x(t) - B_i^{-1} E_i \hat{S}(t)$, where $\hat{S}(t)$ is the adaptive estimation of the fault, and is updated in the following form:

$$\dot{\hat{S}}(t) = E_i P x(t). \tag{32}$$

Theorem 2. *For the closed-loop system (10), if there exists a symmetric positive definite matrix $P = P^T > 0$, scalars $\mu > 0$, $\gamma_0 > 0$ and a control gain matrix K_i such that*

$$\begin{bmatrix} \varphi_1 & PD_i & \theta P & C_i^T \\ * & -{\gamma_0}^2 I & 0 & 0 \\ * & * & -\frac{1}{\mu} I & 0 \\ * & * & * & -I \end{bmatrix} < 0, \tag{33}$$

where $\varphi_1 = (A_i - B_iK_i)^T P + P(A_i - B_iK_i) + \mu I$*, then the closed loop system is said to be asymptotically stable and has* H_∞ *performance index not greater than* γ_0.

Proof.

Case 1. For the i-th subsystem of system (10), when $S(t) = 0$, i.e., $fault = 0$, the Lyapunov function is constructed as follows:

$$V_i(t) = x^T(t)Px(t). \tag{34}$$

By choosing the fault-tolerant control law $u(t) = u_w(t) = -K_ix(t)$, one can get

$$\begin{aligned}
&\dot{V}_i(t) + y^T(t)y(t) - {\gamma_0}^2\omega^T(t)\omega(t)\\
&\quad = \dot{x}^T(t)Px(t) + x^T(t)P\dot{x}(t) + y^T(t)y(t)\\
&\qquad - {\gamma_0}^2\omega^T(t)\omega(t)\\
&\quad = [A_ix(t) + B_iu(t) + D_i\omega(t) + f_i(t,x)]^T Px(t)\\
&\qquad + y^T(t)y(t) - {\gamma_0}^2\omega^T(t)\omega(t) + x^T(t)P[A_ix(t)\\
&\qquad + B_iu(t) + D_i\omega(t) + f_i(t,x)].
\end{aligned} \tag{35}$$

■

According to Lemmas 2 and 3 and Assumption 2, it can be obtained that

$$2x^T(t)Pf_i(x,t) \le \frac{\theta^2}{\mu}x^T(t)P^TPx(t) + \mu x^T(t)x(t), \tag{36}$$

$$\begin{aligned}
2x^T(t)PD_i\omega(t) \le{}& \frac{1}{{\gamma_0}^2}x^T(t)PD_i{D_i}^TPx(t)\\
&+ {\gamma_0}^2\omega^T(t)\omega(t).
\end{aligned} \tag{37}$$

Substituting into Eqns. (37) and (38) yields

$$\begin{aligned}
&\dot{V}_i(t) + y^T(t)y(t) - {\gamma_0}^2\omega^T(t)\omega(t)\\
&\quad \le x^T(t)[(A_i - B_iK_i)^TP + P(A_i - B_iK_i)]x(t)\\
&\qquad + \frac{1}{{\gamma_0}^2}x^T(t)PD_i{D_i}^TPx(t) + {\gamma_0}^2\omega^T(t)\omega(t)\\
&\qquad + \frac{\theta^2}{\mu}x^T(t)P^TPx(t) + \mu x^T(t)x(t)\\
&\qquad + x(t)^T{C_i}^TC_ix(t) - {\gamma_0}^2\omega^T(t)\omega(t)\\
&\quad = x^T(t)[(A_i - B_iK_i)^TP + P(A_i - B_iK_i)\\
&\qquad + {C_i}^TC_i + \frac{1}{{\gamma_0}^2}PD_i{D_i}^TP + \mu I]x(t)\\
&\quad = x^T(t)\Xi x(t)
\end{aligned} \tag{38}$$

Based on the Schur complement, the matrix A can be equated to

$$\Xi = \begin{bmatrix} \varphi_1 & PD_i & \theta P & C_i^T \\ * & -\gamma_0^2 I & 0 & 0 \\ * & * & -\frac{1}{\mu}I & 0 \\ * & * & * & -I \end{bmatrix}, \tag{39}$$

where $\varphi_1 = (A_i - B_iK_i)^TP + P(A_i - B_iK_i) + \mu I$. Therefore, if there is no fault in the system, i.e., when the fault signal $fault = 0$, the closed-loop system (10) is asymptotically stable if $\Xi < 0$ holds and the H_∞ performance index is not greater than γ_0.

Case 2. The actuator fault error function is defined as follows:

$$e_f(t) = S(t) - \hat{S}(t). \tag{40}$$

For the i-th subsystem of system (10), when$S(t) \neq 0$, i.e., $fault = 1$, the Lyapunov function is constructed as follows:

$$\tilde{V}_i(t) = x^T(t)Px(t) + {e_f}^T(t)e_f(t). \tag{41}$$

By choosing the fault-tolerant control law

$$u(t) = u_w(t) + u_s(t) = -K_ix(t) - {B_i}^{-1}E_i\hat{S}(t),$$

one can get

$$\begin{aligned}
\dot{\tilde{V}}_i(t) ={}& \dot{x}^T(t)Px(t) + x^T(t)P\dot{x}(t) + \dot{{e_f}}^T(t)e_f(t)\\
&+ {e_f}^T(t)\dot{e_f}(t)\\
={}& [(A_i - B_iK_i)x(t) - E_i\hat{S}(t) + E_iS(t) + D_i\omega(t)\\
&+ f_i(t,x)]^TPx(t) + x^T(t)P[(A_i - B_iK_i)x(t)\\
&- E_i\hat{S}(t) + E_iS(t) + D_i\omega(t) + f_i(t,x)]\\
&+ x^T(t)P{E_i}^Te_f(t) + {e_f}^T(t)E_iPx(t).
\end{aligned} \tag{42}$$

Substituting into (32) and (41) yields

$$\begin{aligned}
&\dot{\tilde{V}}_i(t) + y^T(t)y(t) - {\gamma_0}^2\omega^T(t)\omega(t)\\
&\quad \le x^T(t)[(A_i - B_iK_i)^TP + P(A_i - B_iK_i)]x(t)\\
&\qquad + 2x^T(t)PD_i\omega(t) + 2x^T(t)PD_i\omega(t)\\
&\qquad + [C_ix(t)]^TC_ix(t) - {\gamma_0}^2\omega^T(t)\omega(t).
\end{aligned} \tag{43}$$

From (37) and (38), one can get

$$\begin{aligned}
&\dot{\tilde{V}}_i + y^T(t)y(t) - {\gamma_0}^2\omega^T(t)\omega(t)\\
&\quad \le x^T(t)[(A_i - B_iK_i)^TP + P(A_i - B_iK_i)]x(t)\\
&\qquad + \frac{1}{{\gamma_0}^2}x^T(t)PD_i{D_i}^TPx(t) + {\gamma_0}^2\omega^T(t)\omega(t)\\
&\qquad + \frac{\theta^2}{\mu}x^T(t)P^TPx(t) + \mu x^T(t)x(t)\\
&\qquad + x(t)^T{C_i}^TC_ix(t) - {\gamma_0}^2\omega^T(t)\omega(t)\\
&\quad = x^T(t)[(A_i - B_iK_i)^TP + P(A_i - B_iK_i)\\
&\qquad + {C_i}^TC_i + \frac{1}{{\gamma_0}^2}PD_i{D_i}^TP + \mu I]x(t)\\
&\quad = x^T(t)\Xi x(t).
\end{aligned} \tag{44}$$

Therefore, as in Case 1, if a fault occurs in the system, i.e., when the fault signal $fault = 1$, the closed-loop system

(10) is asymptotically stable if $\Xi < 0$ is established, and has an H_∞ performance index not larger than γ_0. The proof is complete.

5. Experimental simulation

In order to verify the validity of the design, the morphing aircraft system with variable wing curvature used by Zhu and Yu (2022) is simulated under the influence of external disturbances, actuator faults and uncertainties. The specific model is represented as follows:

$$\begin{cases} \dot{x}(t) = A_\sigma x(t) + B_\sigma u(t) + E_\sigma S(t) \\ \qquad\quad + f_\sigma(x,t) + D_\sigma \omega(t), \\ y(t) = C_\sigma x(t), \end{cases}$$

where

$$\begin{aligned} x(t) &= [x_1(t), x_2(t), x_3(t), x_4(t)]^T \\ &= [\Delta V_0, \Delta\beta_0, \Delta\theta_0, \Delta q_0]^T. \end{aligned}$$

Assuming that the flight conditions of the morphing aircraft are at an altitude of 1.5 km and an air temperature of 300 K. The wing curvature c is considered to be 0% and 1%, i.e., the initial base airfoil state and the system states of the wing curvature $c = 0\%$ and $c = 1\%$ are composed of a morphing aircraft system with two subsystems.

The stability is then verified by simulation, and the relevant matrix parameters are chosen as follows:

$$A(c) = \begin{bmatrix} -0.0003282c - 0.00246 & & & \\ -0.0003766c - 0.000067 & & & \\ 0 & & & \\ 0.00821c + 0.005878 & & & \\ & 3.08c - 3.903 & -9.80 & \\ & -0.000164c - 0.9465 & 0 & 1 \\ & 0 & 0 & 1 \\ & -4.6677 & 0 & 0 \end{bmatrix}.$$

$A(c)$ is the state matrix of the morphing aircraft model with the wing curvature change parameter c. The aircraft increases the wing curvature c by increasing the thickness of the upper surface of the wing, and the change of the state quantity caused by the wing curvature c changes the flight state:

$$A_1 = A(0) = \begin{bmatrix} -0.00246 & -3.903 & -9.8 & 0 \\ -0.000067 & -0.9465 & 0 & 1 \\ 0 & 0 & 0 & 1 \\ 0.005878 & -4.6677 & 0 & 0 \end{bmatrix},$$

$$B_1 = \begin{bmatrix} 0 & 0.0127 & 0 & 0 \\ -0.0596 & 0 & 0 & 0 \\ 0 & 0 & 0.1 & 0 \\ -21.45 & 0 & 0 & 0.1 \end{bmatrix},$$

$$A_2 = A(1) = \begin{bmatrix} -0.002788 & -0.823 & -9.8 & 0 \\ -0.0004366 & -0.9465 & 0 & 1 \\ 0 & 0 & 0 & 1 \\ 0.014088 & -4.6677 & 0 & 0 \end{bmatrix},$$

$$B_2 = \begin{bmatrix} 0 & 0.0127 & 0 & 0 \\ -0.0596 & 0 & 0 & 0 \\ 0 & 0 & 0.1 & 0 \\ -21.45 & 0 & 0 & 0.1 \end{bmatrix},$$

$$C_1 = C_2 = \begin{bmatrix} 1 & 1 & 0 & 0 \\ 0 & 0 & 1 & 1 \end{bmatrix},$$

$$D_1 = D_2 = \begin{bmatrix} 0.5 \\ 0.5 \\ -0.5 \\ -0.5 \end{bmatrix},$$

$$E_1 = \begin{bmatrix} 1 & 0 & 0 & 0 \\ 0 & 0.1 & 0 & 0 \\ 0 & 0 & 0.9 & 0 \\ 0 & 0 & 0 & 0.1 \end{bmatrix},$$

$$E_2 = \begin{bmatrix} 1 & 0 & 0 & 0 \\ 0 & 0.5 & 0 & 0 \\ 0 & 0 & 1 & 0 \\ 0 & 0 & 0 & -0.1 \end{bmatrix}.$$

Since A_1, A_2 are not nonnegative matrices, the interval observer (12) is designed after transforming the system accordingly by choosing nonnegative matrices Ψ and Q:

$$\Psi = \begin{bmatrix} 0.27 & 0 & 0 & 0 \\ 0 & 0.11 & 0 & 0 \\ 0 & 0 & 0.61 & 0 \\ 0 & 0 & 0 & 0.14 \end{bmatrix}, \quad Q = \begin{bmatrix} 1 & 0 \\ 0 & 1 \\ 1 & 1 \\ 0 & 1 \end{bmatrix}.$$

Sylvester's equation in (24) is solved to obtain

$$L_1 = \begin{bmatrix} -0.5827 & 2.6676 \\ 0.1825 & -2.6547 \\ 0.0217 & -11.7344 \\ -0.0076 & 10.0566 \end{bmatrix},$$

$$L_2 = \begin{bmatrix} -0.7436 & 3.1860 \\ 0.3298 & -3.0783 \\ 0.0591 & -11.6556 \\ -0.0246 & 9.9910 \end{bmatrix},$$

$$T_1 = \begin{bmatrix} 86.4427 & 199.4556 & 10.7975 & 46.4861 \\ 0.2419 & 0.5846 & -0.2602 & -0.1005 \\ -2.5021 & -2.5403 & -0.6551 & -0.6490 \\ 0.3319 & 0.7089 & 0.5994 & 0.9119 \end{bmatrix},$$

$$T_2 = \begin{bmatrix} 108.5924 & 353.9227 & 12.8313 & 79.5931 \\ 0.1275 & 0.4338 & -0.2734 & -0.1389 \\ -3.1387 & -4.5024 & -0.6951 & -1.0676 \\ 0.1620 & 0.4840 & 0.5749 & 0.8550 \end{bmatrix}.$$

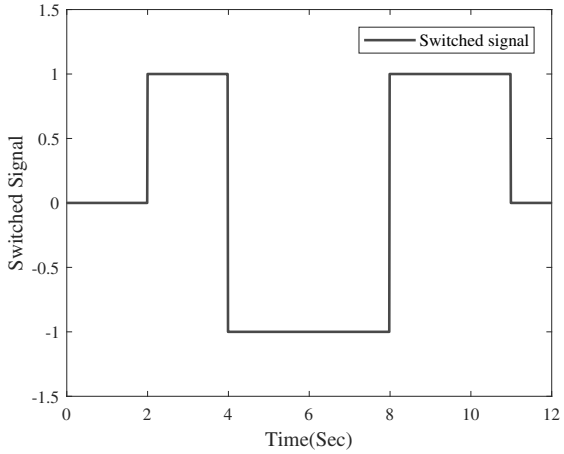

Fig. 1. Curve of switched signal $\sigma(t)$.

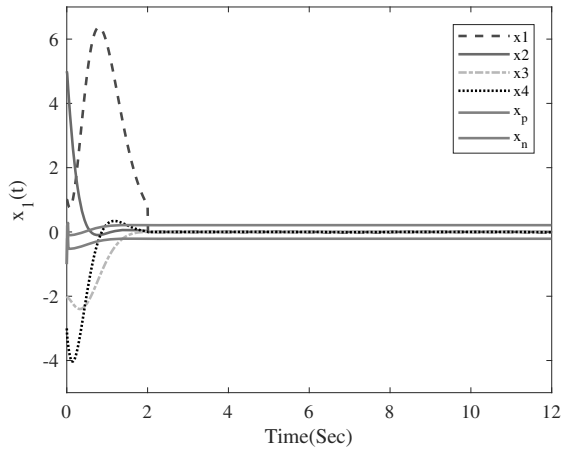

Fig. 2. State interval estimation for subsystem 1.

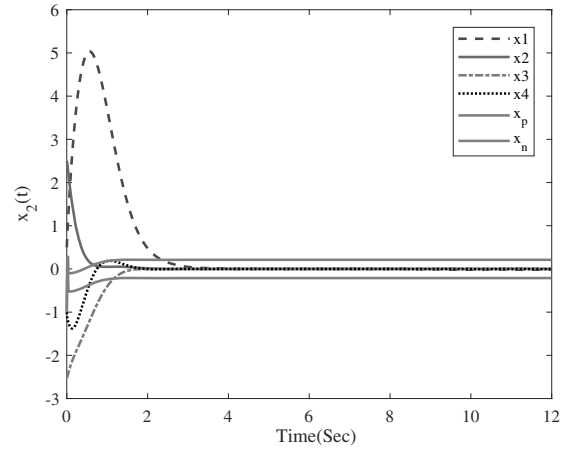

Fig. 3. State interval estimation for subsystem 2.

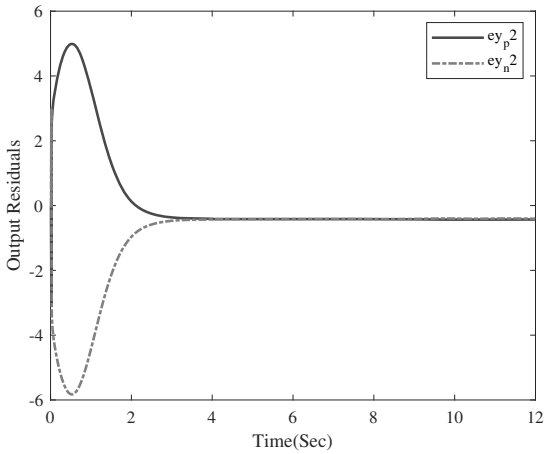

Fig. 4. Residual interval for subsystem 1.

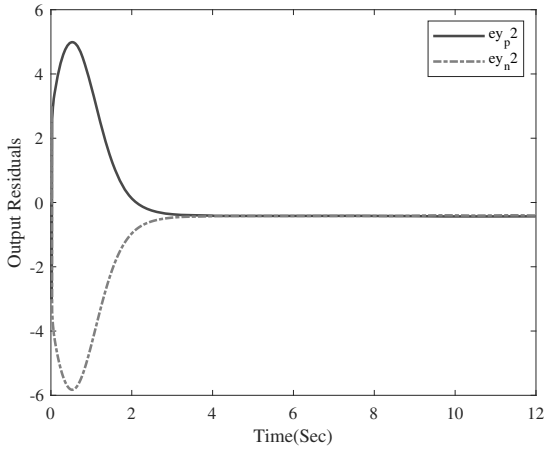

Fig. 5. Residual interval for subsystem 2.

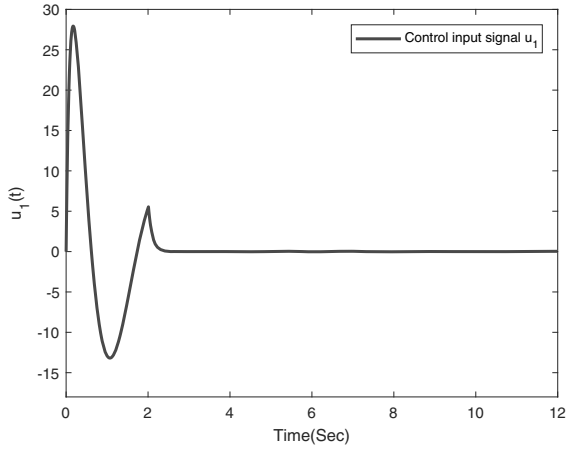

Fig. 6. Control input curve for subsystem 1.

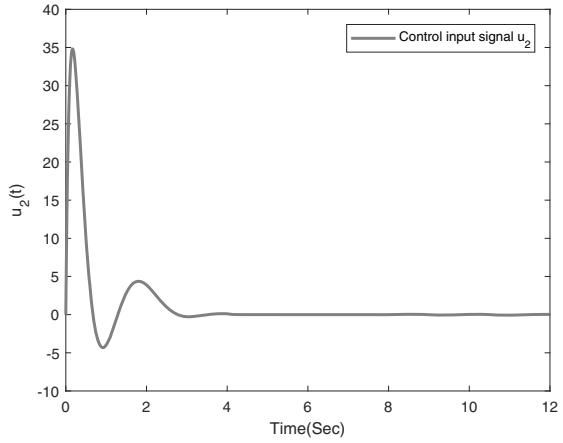

Fig. 7. Control input curve for subsystem 2.

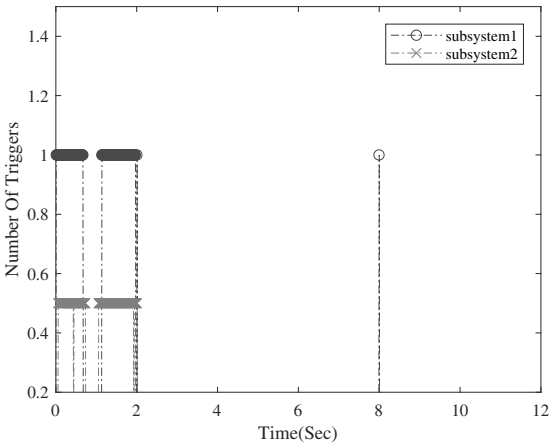

(a) Dynamic event-triggered mechanism.

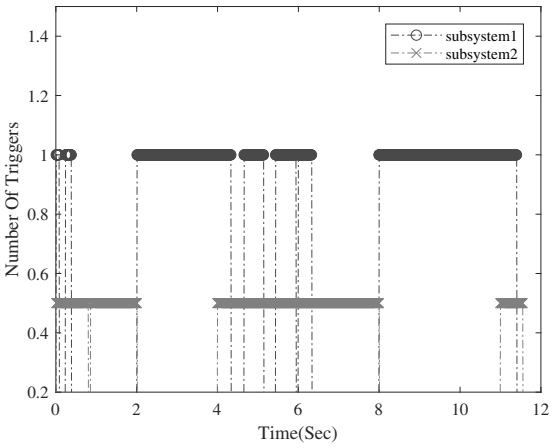

(b) Static event-triggered mechanism.

Fig. 8. Number of triggers for dynamic event triggered and static event triggered mechanisms.

Based on Theorem 2, the control gain matrix of the robust fault-tolerant controller can be obtained as follows:

$$K_1 = \begin{bmatrix} -0.0083 & -41.9500 & -0.0825 & -0.2541 \\ 196.5582 & 78.7062 & 0.0077 & -0.2363 \\ -0.0009753 & -0.0492 & 25.0022 & -6.7054 \\ -1.7427 & -8998.416 & -0.9753 & -29.4957 \end{bmatrix},$$

$$K_2 = \begin{bmatrix} -0.0090 & -41.9500 & -0.1776 & -0.0299 \\ 196.5582 & 78.7028 & 0.0456 & -0.1029 \\ -0.0058 & -0.1058 & 25.0022 & -8.3092 \\ -1.9134 & -8998.416 & -19.7622 & 31.4207 \end{bmatrix}.$$

In order to demonstrate the advantages of the proposed dynamic event-triggered robust fault-tolerant control scheme, this section also shows the design results of the robust fault-tolerant control scheme using static event-triggered mechanism for comparison.

Case 1. The actuator faults in the system is defined as follows:

$$S(t) = \begin{cases} 0, & t < 1, \\ a_1 \sin(2\pi \tilde{f} t), & 1 \le t < 6, \\ a_2(1 - e^{-2(t-3)}), & t \ge 6. \end{cases}$$

where $\tilde{f} = 0.6, \quad a_1 = 0.01, \quad a_2 = 0.02$. In addition, let

$$f_1(t, x_1) = b_1 x_1, f_2(t, x_2) = b_1 x_2, \omega = b_1 \cos(2\pi \tilde{f}_1 t),$$

where $f_1 = 0.7, b_1 = 0.01$. Under the initial conditions

$$x_1(0) = \begin{bmatrix} 1 5 -2 -3 \end{bmatrix}^T,$$

$$x_2(0) = \begin{bmatrix} 0.5 2.5 -2.5 -1 \end{bmatrix}^T,$$

$$\phi_0 = 0,$$

the simulation results are shown in Figs. 1–7.

The switched signal $\sigma(t)$ is shown in Fig. 1. To evaluate the robustness of the proposed H_∞ control framework, the H_∞ performance index γ_0 is optimized to 0.1 via linear matrix inequalities, ensuring a balance between disturbance attenuation and control conservatism. Under the action of the switched signal, the state response curves of the two subsystems of the morphing aircraft at wing curvature $c = 0\%$ and $c = 1\%$ are shown in Figs. 2 and 3.

The residuals of the system outputs with the upper and lower bounds of the interval observer are shown in Figs. 4 and 5. In this study, a single-actuator fault scenario is employed to clearly demonstrate these control performance characteristics.The control input curves for subsystems 1 and 2 are shown in Figs. 6 and 7.

According to the fault detection mechanism (26), it is known that subsystem 1 is in a faulty state before 2.5 s and subsystem 2 is in a faulty state

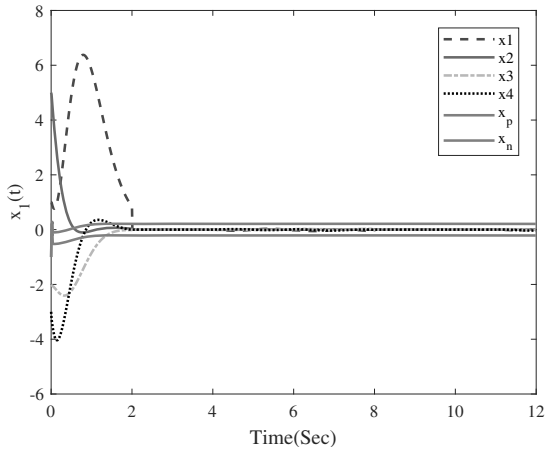

Fig. 9. State interval estimation for subsystem 1.

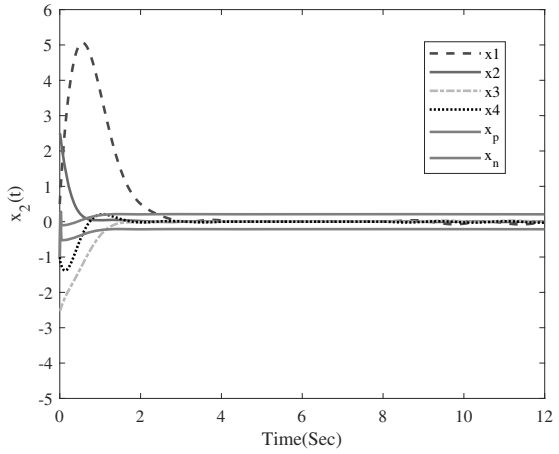

Fig. 10. State interval estimation for subsystem 2.

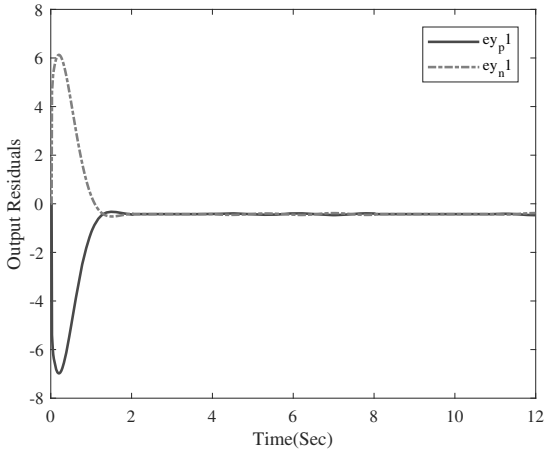

Fig. 11. Residual interval for subsystem 1.

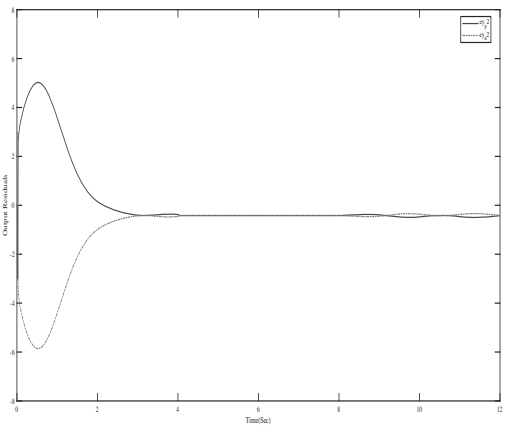

Fig. 12. Residual interval for subsystem 2.

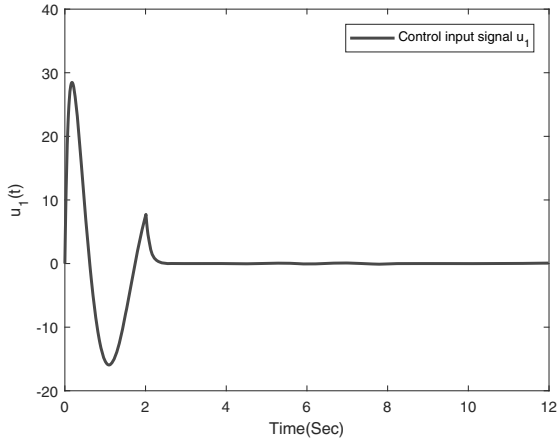

Fig. 13. Control input curve for subsystem 1.

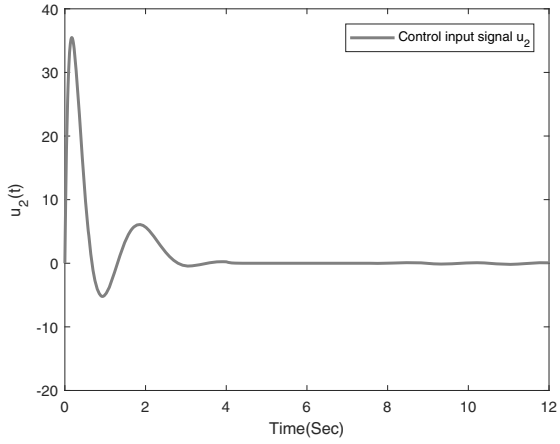

Fig. 14. Control input curve for subsystem 2.

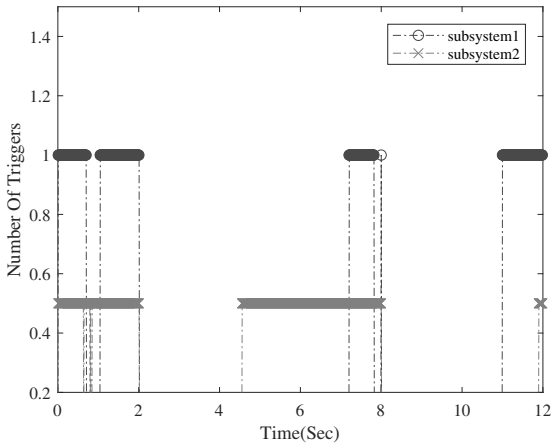

(a) Dynamic event-triggered mechanism.

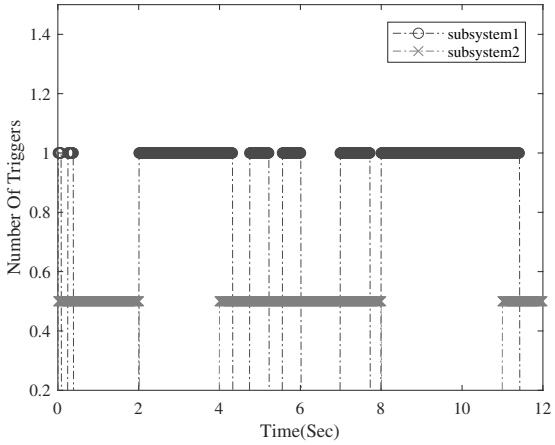

(b) Static event-triggered mechanism.

Fig. 15. Number of triggers for dynamic event triggered and static event triggered mechanisms.

before 4 s. Based on the designed fault-tolerant control law, the effects of disturbances and actuator failures are effectively compensated,enabling the system state to quickly converge to 0 and achieve asymptotic stability with prescribed H_∞ performance ($\gamma_0 = 0$), while effectively suppressing external disturbances and model uncertainties.

When the event-triggered mechanism is not used, the number of data transfers for 12 s of system operation reaches 1200 times. As shown in Fig. 8(b), under the static event-triggered mechanism, the data of the two subsystems are transmitted 731 and 653 times respectively, which are about 39.1% and 45.6% less than the total number of transmissions respectively. As shown in Fig. 8(a), under the dynamic event-triggered mechanism, the data of the two subsystems are transmitted 153 times and 162 times, respectively, which are about 87.3% and 86.5% less than the total number of transmissions, respectively. Compared with the static event-triggered mechanism, the number of data transmissions is reduced by about 40.9 to 48.2% through the dynamic event-triggered mechanism while ensuring the desired performance of the system, and communication and computation resources are effectively saved.

Case 2. The actuator faults in the system is defined as follows:

$$S(t) = \begin{cases} 0, & t < 1.5, \\ a_3 \sin(2\pi \tilde{f} t), & 1.5 \le t < 6, \\ a_4(1 - e^{-2(t-3)}), & t \ge 6, \end{cases}$$

where $\tilde{f} = 0.6, a_3 = 0.05, a_4 = 0.1$. In addition, let

$$f_1(t, x_1) = b_1 x_1, f_2(t, x_2) = b_1 x_2, \omega = a_3 \sin(2\pi \tilde{f} t),$$

where $\tilde{f}_1 = 0.7, b_1 = 0.1$.

By enhancing the amplitude of disturbances and faults, the state response curves of subsystem 1 and subsystem 2 are shown in Figs. 9 and 10, and the output residual intervals are shown in Figs. 11 and 12. The control input curves for subsystem 1 and 2 are shown in Figs. 13 and 14. It can be seen that the system still converges quickly and with good performance.

It can be seen that the system still converges quickly and with good performance. In this scenario, as shown in Fig. 15(b), under the static event-triggered mechanism, the data of the two subsystems are transmitted 765 and 702 times, respectively, which is 36.3% and 41.5% less than the total number of transmissions, respectively. As shown in Fig. 15(a), the data of the two subsystems under the dynamic event-triggered mechanism are transmitted 330 and 491 times, respectively, which are 72.5% and 59.1% less than the total number of transmissions, and could be reduced by about 17.6% to 36.2% compared with the static event-triggered mechanism.

As shown in the simulation results, the interval observer-based fault detection mechanism designed in this paper can intuitively determine the fault conditions. When the fault is identified, the robust fault-tolerant controller based on the dynamic event-triggered mechanism can make the variable wing curvature morphing aircraft system reach stability and maintain good robustness, and effectively reduce the consumption of communication and computational resources.

6. Conclusion

In this paper, the problem of control system design for a class of morphing aircraft with variable wing curvature is investigated. Firstly, the transformation

process of the morphing aircraft is modelled as a nonlinear switched system with uncertainty and subject to both external disturbances and actuator faults. Secondly, the interval observer-based fault detection method and the dynamic event-triggered robust fault-tolerant control strategy are studied. The upper and lower bounds of the system output without actuator faults are constructed by designing interval observers, and the occurrence of faults is intuitively identified according to whether the actual system output exceeds this range. Thirdly, a dynamic event-triggered robust fault-tolerant control scheme is designed, in which two different controllers are used for switching control according to the real-time fault detection results. It ensures the boundedness of the signal of the closed-loop system, and effectively reduces the number of data transmission and saves communication resources. Finally, the gain matrices of the observer and controller can be obtained by solving Sylvester's equation and linear matrix inequality through MATLAB, respectively. The designed fault diagnosis mechanism and fault-tolerant control method are applied to a nonlinear model of a morphing aircraft system with variable wing curvature, and the effectiveness of the designed fault detection mechanism and control method is verified.

Acknowledgment

This work is supported by the National Natural Science Foundation of China under the grant 62103057. The authors declare no conflict of interest.

References

Abbaspour, A., Aboutalebi, P., Yen, K.K. and Sargolzaei, A. (2017). Neural adaptive observer-based sensor and actuator fault detection in nonlinear systems: Application in UAV, *ISA Transactions* **67**: 317–329.

Ashraf, M.A., Ijaz, S., Javaid, U., Hussain, S., Anwaar, H. and Marey, M. (2021). A robust sensor and actuator fault tolerant control scheme for nonlinear system, *IEEE Access* **10**: 626–637.

Avram, R.C., Zhang, X. and Muse, J. (2017). Quadrotor actuator fault diagnosis and accommodation using nonlinear adaptive estimators, *IEEE Transactions on Control Systems Technology* **25**(6): 2219–2226.

Cui, D. and Xiang, Z. (2022). Nonsingular fixed-time fault-tolerant fuzzy control for switched uncertain nonlinear systems, *IEEE Transactions on Fuzzy Systems* **31**(1): 174–183.

Ding, D., Wang, Z. and Han, Q.-L. (2019). A set-membership approach to event-triggered filtering for general nonlinear systems over sensor networks, *IEEE Transactions on Automatic Control* **65**(4): 1792–1799.

Dong, C., Jiang, W. and Wang, Q. (2015). Smooth switching LPV robust H_∞ control for variable-span vehicle, *Journal of Astronautics* **36**(11): 1270–1278.

Germán-Salló, Z. and Strnad, G. (2018). Signal processing methods in fault detection in manufacturing systems, *Procedia Manufacturing* **22**: 613–620.

Girard, A. (2014). Dynamic triggering mechanisms for event-triggered control, *IEEE Transactions on Automatic Control* **60**(7): 1992–1997.

Guo, S. and Zhu, F. (2016a). Actuator fault detection based on interval observers, *Control and Decision* **31**(6): 5.

Guo, S. and Zhu, F. (2016b). Interval observers design for descriptor systems, *Control and Decision* **31**(2): 6.

Guo, S., Zhu, F. and Li, Z. (2019). Actuator fault detection for descriptor system: An interval observer approach, *Control Engineering of China* **36**(11): 6.

Habibi, H., Howard, I. and Simani, S. (2019). Reliability improvement of wind turbine power generation using model-based fault detection and fault tolerant control: A review, *Renewable Energy* **135**: 877–896.

Junnila, V. and Laihonen, T. (2020). Tolerant location detection in sensor networks, *Advances in Applied Mathematics* **112**: 101938.

Li, J., Pan, K., Zhang, D. and Su, Q. (2019). Robust fault detection and estimation observer design for switched systems, *Nonlinear Analysis: Hybrid Systems* **34**: 30–42.

Li, P., Zhao, X., Qin, H., Wang, Z. and Niu, B. (2021). Dynamic event-triggered finite-time H_∞ tracking control of switched LPV aero-engine models, *IEEE Transactions on Circuits and Systems II: Express Briefs* **69**(3): 1114–1118.

Lian, J. and Li, C. (2021). Event-triggered adaptive tracking control of uncertain switched nonlinear systems, *International Journal of Robust and Nonlinear Control* **31**(9): 4154–4169.

Liang, X., Wang, Q. and Dong, C. (2019). Robust adaptive control for morphing aircraft based on switching system, *Journal of Beijing University of Aeronautics and Astronautics* **45**(3): 538–545.

Ligang, G., Qing, W., Changhua, H. and Chen, L. (2020). Switching control of morphing aircraft based on Q-learning, *Chinese Journal of Aeronautics* **33**(2): 672–687.

Liu, X., Su, X., Shi, P., Nguang, S.K. and Shen, C. (2019). Fault detection filtering for nonlinear switched systems via event-triggered communication approach, *Automatica* **101**: 365–376.

Long, L., Wang, F. and Chen, Z. (2022). Robust adaptive dynamic event-triggered control of switched nonlinear systems, *IEEE Transactions on Automatic Control* **68**(8): 4873–4887.

Ma, H., Li, H., Lu, R. and Huang, T. (2020). Adaptive event-triggered control for a class of nonlinear systems with periodic disturbances, *Science China Information Sciences* **63**(5): 1–15.

Meng, X., Zhai, D., Fu, Z. and Xie, X. (2020). Adaptive fault tolerant control for a class of switched nonlinear systems with unknown control directions, *Applied Mathematics and Computation* **370**: 124913.

Wan, X., Han, T., An, J. and Wu, M. (2021). Fault diagnosis for networked switched systems: An improved dynamic event-based scheme, *IEEE Transactions on Cybernetics* **52**(8): 8376–8387.

Wang, R., Hou, L., Zong, G., Fei, S. and Yang, D. (2019). Stability and stabilization of continuous-time switched systems: A multiple discontinuous convex Lyapunov function approach, *International Journal of Robust and Nonlinear Control* **29**(5): 1499–1514.

Wu, Y., Zhang, J. and Fu, S. (2021). Non-fragile event-triggered control of positive switched systems with random nonlinearities and controller perturbations, *Bulletin of the Polish Academy of Sciences: Technical Sciences* **69**(5), Article no. e138566.

Wu, Z., Lu, J., Zhou, Q. and Shi, J. (2017). Modified adaptive neural dynamic surface control for morphing aircraft with input and output constraints, *Nonlinear Dynamics* **87**(4): 2367–2383.

Xia, D. and Fu, X. (2024). Observer-based sliding-mode fault-tolerant consistent control for hybrid event-triggered multi-agent systems, *International Journal of Applied Mathematics and Computer Science* **34**(3): 361–373, DOI: DOI: 10.61822/amcs-2024-0026.

Yang, G. and Zhang, Z. (2018). Review of interval observer based fault diagnosis techniques for dynamic systems, *Control and Decision* **33**(5): 13.

Zhao, X., Zhang, L., Shi, P. and Liu, M. (2011). Stability and stabilization of switched linear systems with mode-dependent average dwell time, *IEEE Transactions on Automatic Control* **57**(7): 1809–1815.

Zhu, Z. and Yu, J. (2022). *Anti-disturbance Control of Switching System and its Application in Variant Aircraft*, Master's thesis, Yangzhou University, Yangzhou.

XingJian Fu received his PhD in the School of Automation, University of Science and Technology Beijing, China, in 2005. Currently, he is a professor at Beijing Information Science and Technology University. He has published about 100 papers. He is a committee member of the Mechanical Industry Automation Branch of the China Mechanical Engineering Society, as well as a member of the China Automation Society and of the Chinese Association for Artificial Intelligence. His research interests include intelligent control, robust fault-tolerant control and moving body control.

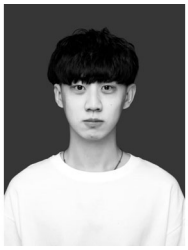

XiaoHan Wang received his BS degree in engineering from the Qingdao Institute of Technology in 2021, and is currently pursuing his MS degree in the School of Automation, Beijing Information Science and Technology University (BISTU). His research interests include fault-tolerant control strategies for nonlinear switched systems and event-triggered mechanisms.

Received: 13 November 2024
Revised: 25 February 2025
Re-revised: 17 April 2025
Accepted: 23 April 2025